

Observed year-to-year sea surface salinity variability in the Bay of Bengal during the 2009 – 2014 period

Chaitanya A.V.S.¹, F. Durand^{2,3}, S. Mathew⁴, V.V. Gopalakrishna¹, F. Papa^{2,3}, M. Lengaigne^{5,6}, J. Vialard⁵, Ch. Kranthikumar¹ and R. Venkatesan⁴

- (1) CSIR/National Institute of Oceanography (NIO), Goa, India
- (2) IRD/Laboratoire d'études en Géophysique et Océanographie Spatiales (LEGOS), Toulouse, France
- (3) Indo-French Cell for Water Sciences, IISc-NIO-IITM-IRD Joint International Laboratory, IISc, Bangalore, India
- (4) National Institute of Ocean Technology (NIOT), Chennai, India
- (5) Sorbonne Universités, UPMC Univ Paris 06, UMR 7159, LOCEAN, F-75005, Paris, France
- (6) Indo-French Cell for Water Sciences, National Institute of Oceanography, Dona Paula, India

Abstract

The present study describes the observed sea surface salinity (SSS) interannual variability in the Bay of Bengal over the 2009-2014 period. It is based on an original compilation of all available in situ SSS observations in that region, assembled in a 2°-resolution trimonthly gridded field. We find that year-to-year SSS variability is particularly strong in the North-Eastern part of the Bay. Over recent years, this variability takes the form of two successive and opposite phases: a saltening phase from mid-2009 to late 2010, immediately followed by a freshening phase from late 2010 to late 2011. The typical magnitude of each anomalous spell is about one in the practical salinity scale, making this area one of the most variable of the tropical oceans at interannual timescales. A simple mixed-layer salt budget indicates that year-to-year large-scale SSS variability in the Northern Bay of Bengal is primarily driven by freshwater fluxes variability with a correlation of 0.68, with rather independent contributions from precipitation and river runoff. The oceanic surface circulation variability contributes less systematically to the large-scale SSS evolution in the Northern Bay of Bengal over the entire record with a correlation of 0.13, despite a strong contribution at times, in particular during the 2011 positive Indian Ocean Dipole (IOD) freshening.

Keywords: SSS, Bay of Bengal, Argo, Ganges, Brahmaputra, IOD

1 Introduction

The Bay of Bengal (henceforth BoB) forms the northeastern part of the Indian Ocean and is blocked by landmasses to the north of 23°N. Ocean currents within this semi-enclosed basin are strongly influenced by the seasonally-reversing monsoon winds. This basin is also the recipient of intense precipitation and continental river runoff, with most of the freshwater flux entering the northern half of the basin during summer monsoon and post-monsoon season. The yearly freshwater flux received by the BoB largely exceeds the freshwater flux evaporated back to the atmosphere (Shenoi et al. 2002; Sengupta et al. 2006). As a result, sea surface salinity (SSS) is consistently very low in the northern BoB (typically inferior to 32¹). This low SSS in the BoB is thought to have various implications for regional climate through its stabilizing effect of the water column. These fresh surface waters indeed maintain shallow mixed layers in the Bay, which are efficiently warmed by surface heat fluxes (e.g. de Boyer Montégut et al. 2007). They are thus held responsible for the consistently high sea surface temperature (SST) in the BoB, compared to the neighbouring tropical basins (Han et al. 2001; Shenoi et al. 2002; Rao et al. 2002a; Girishkumar et al. 2013). As the SST is often above the critical threshold of 28°C (considered as the limit above which deep atmospheric convection can develop, e.g. Gadgil et al. 1984), the BoB is prone to intense air-sea interactions. A well-known manifestation of these is the development of tropical depressions and cyclones over the Bay, which intensity could be partly controlled by this salinity stratification. These salt-stratified waters indeed inhibit vertical mixing under tropical cyclones and reduce the resulting surface cooling (Sengupta et al. 2008, Neetu et al. 2012), therefore promoting an intense surface evaporation that contributes to the cyclones intensification. This control of upper ocean temperature by BoB salinity stratification is not limited to the influence of tropical cyclones, but also occurs at longer timescales. Two recent studies indeed suggested that intraseasonal SST variability in the Northern BoB could be modulated by salinity stratification (Vinayachandran et al. 2012, Girishkumar et al. 2013). These influences of upper ocean salinity on surface temperature, and potentially on the atmosphere, call for an in-depth description of the SSS spatial and temporal variability within the Bay.

The seasonal cycle of BoB salinity was first analysed in the study of Rao and Sivakumar (2003). It is displayed on Figure 1, based on the North Indian Ocean Atlas (NIOA) of Chatterjee et al. (2012). The strongest seasonal variations occur in the northern part of the basin. In summer, the freshest surface waters (SSS below 32) occupy the northernmost part of the basin (to the north of 18°N). With the advent of the summer monsoon, the freshwater supply into the bay ramps up. As the

¹ Salinity is expressed in the Practical Salinity Scale throughout this paper, i.e. in grams of salt per kilogram of seawater, hence without units.

precipitation maximum and dominant river outlets are both located in the northern BoB, salinity starts decreasing there. By fall, the 32 isohaline has been displaced southward by several hundreds of kilometers, in particular along the eastern and western boundaries. The southward-flowing ocean boundary currents play a key role in the southward export of the freshwaters during this season (Benshila et al. 2014; Chaitanya et al. 2014; Akhil et al. 2014). These fresh waters start retreating back northward in winter, to reach their minimal extent in spring, with SSS values below 32 seen only at the northern extremity of the basin. The modelling study of Akhil et al. (2014) suggests that vertical mixing of surface fresh waters with underlying saltier waters is the primary driver of this saltening phase.

Beyond this seasonal picture, much less is known about BoB SSS variations at other timescales. At intraseasonal timescales, Parampil et al. (2010) described a substantial variability of mixed-layer salinity based on a few drifting profilers in the central BoB, and suggested that it is mainly driven by small-scale advection of riverine and atmospheric freshwater by ocean turbulent circulation. Rao et al. (2011) also suggested a dominant role of oceanic circulation over air-sea freshwater fluxes on SSS intraseasonal variability in the BoB based on ship-borne hydrographic observations.

The limited coverage of available SSS observations over the BoB has prevented the oceanographic community from assessing SSS variations at longer timescales, and in particular interannual variations. Over the past few years though, the SSS observing system over the BoB has been improving consistently and it has now become possible to monitor the year-to-year basin-scale SSS variations. The objective of the present study is threefold. We first present a novel SSS dataset encompassing the whole BoB, with a pluri-annual time span from 2009 to 2014 (Section 2). We then describe the year-to-year variations of SSS over the northeastern BoB during this period for the first time, based on this dataset (Section 3). The mechanisms driving interannual SSS variability are then discussed using a simple mixed-layer salinity budget (Section 4). Section 5 summarizes our main results and discusses the limitations and perspectives of our study.

2 Methods and datasets

2.1 In situ SSS datasets

Our study is based on an original, comprehensive compilation of all in situ SSS datasets available over the BoB during the 2009-2014 period (from December 2008 to May 2014) (Fig. 2a). It gathers six different salinity data sources: Argo (Array for Real-Time Geostrophic Oceanography; Roemmich et al. 2009) profilers, ship-of-opportunity eXpendable Conductivity-Temperature-Depth (XCTD) profiles and bucket measurements, Research Moored Array for African-Asian-Australian

Monsoon Analysis and Prediction (RAMA) moorings (McPhaden et al. 2009), OMNI moorings (Venkatesan et al. 2013), ship-of-opportunity thermosalinograph transects and dedicated hydrographic cruises. We detail those various data sources below.

The main contributor to our SSS dataset is the Argo database, obtained from the Ifremer Data Centre (<ftp.ifremer.fr/ifremer/argo>). Argo profilers are autonomous drifters that provide temperature and salinity profiles from 2000 m depth to the surface, every 5 to 10 days. The amount of Argo floats drifting in the BoB gradually increased from 30 to 60 over the 2009-2014 period. They yielded between 1200 (in 2009 and 2010) to 4000 (in 2013) yearly salinity profiles (Fig. 2b). We extracted the uppermost valid measurement within the 5 m – 15 m layer, with « good » or « probably good » quality flag (see Argo quality control manual, 2012 available on www.argodatamgt.org/content/download/341/2650/file/argo-quality-control-manual-V2.7.pdf). For most profiles, this uppermost record is typically situated at about 8 m – 9 m depth. We will discuss the influence of the sampling depth on the SSS estimate in section 2.2.

We also considered SSS measurements collected from both bucket samples and XCTD temperature and salinity profiles along two repeated merchant ship tracks between Chennai (label « C » in Figure 2a) and Port Blair (label « PB »), and between Kolkata (label « K ») and Port Blair. 953 bucket measurements and 249 XCTD profiles were collected along the C-PB and K-PB transects over the 2009-2014 period. Along both routes, the spatio-temporal resolution of the bucket samples and XCTD casts varies but remains close to 1° and 2 months, with about 20 such voyages between July 2009 and December 2013 (see Figure 2c for an illustration of the spatio-temporal distribution of the XCTD data collected on the Kolkata - Port Blair transect). The bucket samples were analysed using a Guild Line 8400 Autosol salinometer following standard international procedures. This ensures a typical accuracy of salinity of about 10^{-3} . XCTD salinity records over the upper 4 m were discarded as it is usually done to account for the delay in the conductivity sensor response (e.g. Tanguy et al. 2010) and we considered the 5 m record as SSS.

Three RAMA buoys have been episodically measuring salinity at 1 m depth over the 2009-2014 period, at 90°E-8°N, 90°E-12°N and 90°E-15°N. Data return rates vary between 50% at 8°N and 12°N and 75% at 15°N. We used the 5-day averaged data obtained from the RAMA website (<http://www.pmel.noaa.gov/tao/disdeld/disdeld-rama.html>). Further details on the moorings design and data quality control can be found in McPhaden et al. (2009).

OMNI deep-ocean moorings are similar to RAMA moorings, except that they are inverse catenary mooring. Six moorings were deployed in various regions of the BoB in 2011 (11°N-86.5°E, 8°N-

85.5°E, 14°N-83°E, 16.5°N-88°E, 10.5°N-94°E, 18.2°N-89.7°E) with an average data return of 99%. Data from all sensors are collected during the last 10 minutes of every hour and stored in the internal storage facility. Data received are transmitted to the shore station using INMARSAT geostationary satellite communication every third hour (Venkatesan et al. 2013). Both high- and low-resolution data are archived at the Indian National Centre for Ocean Information Systems (INCOIS) after standard quality control procedures. They are delivered to end users through the Ocean Data Information Systems (ODIS) (Shesu et al. 2013). The Conductivity Temperature (CT) sensors are fitted at 5, 10, 15, 20, 30, 50, 75, 100, 200 and 500 m depth along the mooring line. The CT sensors are Seabird SBE37-IM model with an accuracy of 0.002°C for temperature and 0.003 mS/cm for conductivity. Salinity data at 5 m depth from all the six moorings over mid 2011 to mid 2013 was used in this study.

A merchant ship (M/S Lavender) equipped with a thermosalinograph continuously measuring the near-surface salinity, has been crossing the southern Bay ten times from 2009 through September 2013 (typically once every five months). The thermosalinograph data went through a delayed-mode quality control including comparison with climatology and correction with external water samples. Although it is hard to assign a specific depth to the thermosalinograph measurements (because of varying ship speed and load), the data may be representative of the 0 – 10 m upper ocean layer (see Delcroix et al. 2005 for full details on the data acquisition and processing procedures). A few near-surface measurements from shipborne CTD casts were also made available by the National Institute of Oceanography Data Centre (India). Most of the observations were collected in the coastal western Bay (Fig. 2a), at 0-10 m depth, in 2009-2011.

2.2. Data reduction

The spatio-temporal sampling achieved by these various datasets is very heterogeneous. First, these data originate from different depths within the upper 10 m of the water column, which may induce errors in the estimation of SSS evolution. A vast majority of the salinity data are provided by Argo floats, for which salinity has consistently been measured at a depth close to 8 m. The resulting SSS error has been estimated using data from the 15°N, 90°E RAMA mooring. The root-mean square difference between salinity sampled at 1 and 10 m depth is only 0.17, about four times smaller than the 1 m salinity variations with a standard deviation of 0.63. This difference is also typically much smaller than the ~ 0.5 to 1 SSS signals we analyse in the rest of the study. We checked that the spatial patterns of SSS variability we obtained were not altered when using RAMA 10 m (instead of 1 m) and XCTD 8 m (instead of 5 m) values (not shown). It is therefore unlikely that the varying depth of data collection induces a significant error in our analyses. Second, although our datasets

cover the bulk of the BoB, one has to keep in mind that some sub-regions are left completely unsampled (Fig. 2a; see in particular the Andaman sub-basin between 93°E and the eastern boundary, as well as the far northern bay to the north of 20°N).

In a similar way to de Boyer Montégut et al. (2014), we merged the six datasets by computing the median of all available individual measurements on a $2^\circ \times 2^\circ \times 3$ months grid. This grid cell size was chosen after several trials (not shown), and found to give the best compromise between the resolved scales and actual data coverage. We did not attempt to fill the data gaps in the resulting gridded dataset, to avoid introducing any spurious signal in the merged product. Rather, we simply keep the data-void regions out of our study.

2.3 Freshwater fluxes

In order to quantify the atmospheric and continental control of SSS variability, we have to account for evaporation (E), precipitation (P) and river runoff (R). Daily TropFlux $1^\circ \times 1^\circ$ gridded product (Praveen Kumar et al. 2012) provides the evaporation data. This product is available from 1979 to 2013 (see www.locean-ipsl.upmc.fr/tropflux/ for details) and is largely derived from ERA-Interim re-analysis (Dee et al. 2011) with ad-hoc corrections derived from observations. We used the 3-hourly, $0.25^\circ \times 0.25^\circ$ Tropical Rainfall Measuring Mission (TRMM) 3B42 precipitation gridded product (Huffman et al. 2007) over the 2009 – 2014 period. It is a merged product from multi-satellite and in situ data from rain gauges. This dataset is available from <http://disc.sci.gsfc.nasa.gov/precipitation>. Finally, runoffs from the three largest river systems in the BoB are included in our study: the Brahmaputra, the Ganges and the Irrawaddy (their locations are shown in Fig. 1). For the Ganges-Brahmaputra river system, we use monthly estimates of continental freshwater flux into the BoB from Papa et al. (2012). This time-series is derived from a combination of in situ elevation-discharge relationships (the so-called rating curve, Papa et al., 2010) with river water level retrieved from multiple altimetry satellites (TOPEX/Poseidon, ERS-2, ENVISAT and Jason-2). For the Irrawaddy River, in situ discharge time series are unfortunately not available over the recent period. Furuichi et al. (2009) published monthly estimates from in situ observations over the 1966-1996 period. We used their monthly in situ discharge data, together with TOPEX/Poseidon river level timeseries over their common period of availability (1993-1996) to establish a rating curve following a similar approach to that of Papa et al. (2012). We then used this rating curve to derive a continuous, monthly estimate of the Irrawaddy river discharge at the river mouths for 1993-2012 using TOPEX/Poseidon (1993-2002), ENVISAT (2002-2008) and Jason-2 (2008 onwards).

During the period of the present study (2009 onwards), the estimates of river discharge rely on Jason-2 observations. Note that no runoff data are available after December 2012.

2.4 Surface current

The role of oceanic transports on SSS variability is assessed using OSCAR (Ocean Surface Current Analyses – Real time) surface current product of Bonjean and Lagerloef (2002). This product is a combination of altimetry-derived geostrophic current and Ekman drift from scatterometer wind. This product is available at various spatial and temporal resolutions. In this study we considered the version at $1^\circ \times 1^\circ \times 5$ day, filtered, available from www.oscar.noaa.gov.

3. Observed variability of SSS

Interannual SSS anomalies are first computed by subtracting the seasonal climatology of Chatterjee et al. (2012) from the blended trimonthly multi-year gridded SSS product introduced in Section 2. The standard deviation of these interannual anomalies (Figure 3a) illustrates the contrasted magnitude of interannual SSS variability within the BoB. SSS interannual variability is strongest (above 0.45) in the north-eastern quarter of the basin, and in the coastal strip hugging the western boundary (to the north of 10°N) while it is lowest in the central part of the basin (lower than 0.45). In both regions, the observational coverage is satisfactory with typically more than 50% of the 2009-2014 period covered (Fig. 3b), and more than 4 individual observations per pixel on average (Fig. 3c). The area around 81°E , 15°N , however stands out as a poorly covered region, with 2 to 4 observations per pixel and less than 50% of the seasons monitored. Our SSS product should hence be considered with caution in this area.

Durand et al. (2011) found that the total (seasonal plus interannual) SSS variability in their numerical simulation was also maximum in the northern and western parts of the Bay, and minimal in the central basin. Akhil et al. (2014) also reported strongest seasonal SSS variability close to the northern and western boundaries in their simulation. Our observational product strongly suggests the same spatial distribution at interannual timescales. Durand et al. (2011) further diagnosed that the sole Ganges-Brahmaputra year-to-year discharge changes were able to drive SSS interannual signals of ~ 0.2 restricted to the northernmost part of the basin (north of about 18°N). Our observational product reveals a much stronger interannual variability, with a standard deviation above 0.45 as far south as 14°N . This suggests that other mechanisms than Ganges-Brahmaputra runoff (P, E and/or oceanic circulation) influence SSS interannual variability in the northern half of the Bay. The mechanisms driving the observed SSS interannual evolution will be specifically addressed in the section 4. In the following, we focus our study on the region that displays the most consistent area of

maximum SSS variability: the North-Eastern Bay (henceforth NEB) defined as the 14°N-23°N, 86°E-96°E box (Figure 3a).

Figure 4 displays the NEB average SSS evolution. SSS interannual anomalies in excess of 1 can persist in this relatively large box during several seasons. This magnitude is commensurate with signals observed in other highly variable regions of the tropical oceans, such as the equatorial Indian Ocean (Durand et al. 2013) or the far-eastern equatorial Pacific Ocean (Alory et al. 2012). The observed SSS evolution displays a marked seasonal cycle, with freshening during the monsoon season and saltening during the following winter and spring, in agreement with Chatterjee et al. (2012) climatology. Year-to-year variations mostly consist of a modulation of the monsoonal freshening magnitude. This freshening is stronger than normal in 2011 and 2013, resulting in fresh anomalies during the post-monsoon season (down to -0.5 in SON 2011 and -0.9 in SON 2013). Conversely, the monsoonal freshening is weaker than normal in 2010, resulting in a +1 salty anomaly in SON 2010. 2009 is also characterized by a change in the timing of the monsoonal freshening, which starts three months earlier than in the seasonal climatology. As a result, the NEB is anomalously fresh during the 2009 monsoon (-0.5 anomaly in JJA 2009). Recent interannual SSS variations in the NEB can thus be described as a seesaw between fresher-than-normal conditions (before early 2010 and after late 2011) and saltier-than-normal conditions (in the intervening period).

Figure 5 shows the anomalous SSS patterns derived from our blended product at the height of these anomalous events (JJA 2009, SON 2010, SON 2011 and SON 2013). The salty extreme of SON 2010 appears as a coherent positive SSS anomaly spanning the entire eastern half of the basin, reaching around +1 in the central part of NEB, and with local maxima above +2 in the northern part of NEB (around 90°E, 19°N). The fresh extremes in JJA 2009, SON 2011 and SON 2013 are patchier. This patchiness is particularly obvious for the SON 2013 event, with salty anomalies in the central NEB, co-existing with fresh anomalies in the northern and southern part of NEB. During these three periods SSS anomalies are below -2.5 around 21°N, 89°E. It should be noted that the observational coverage of this northernmost grid point in our product consists only of one to two ship-of-opportunity transects over each trimonthly period, so that the gridded value we estimate may have a significant level of uncertainty due to aliasing of unresolved high-frequency variability.

The saltier-than-normal phase lasts almost two years (from late 2009 to mid 2011), which is much longer than the few months typical lifetime of interannual anomalies driven by Ganges-Brahmaputra river runoff in the model simulations of Durand et al. (2011). This motivated us to jointly consider all the possible freshwater forcing fluxes contributing to SSS anomalies: runoff of course, but also precipitation and evaporation through air-sea interface. Figure 6 shows the corresponding evolution

of the three components of the freshwater flux (E, P and R) integrated over the NEB domain. This figure first illustrates that the evaporation flux exhibits little departure from its seasonal climatology, over most of the period. The precipitation and runoff fluxes both display a similar seasonal evolution with high precipitation and large runoff during the summer monsoon and low freshwater supply during winter and spring. Largest precipitation and runoff year-to-year variability occur during and shortly after the monsoon. Year-to-year precipitation and runoff anomalies do not always vary in phase. In 2009 for instance, precipitation is close to normal, whereas discharge is deficient. On the contrary, in 2010, precipitation is deficient, whereas discharge is above normal. This may be linked to the displacement of the atmospheric convective zone from the Northern Bay to North-Western India during the abnormal monsoon of 2010 (Mujumdar et al. 2012). Positive precipitation anomalies over the Ganges watershed indeed induce positive discharge anomalies at the river mouths with a lag of about 2 weeks (Jian et al. 2009). In 2011, both precipitation and runoff are above normal. In 2012, precipitation is also above normal, but runoff is close to normal. In 2013, precipitation is above normal and runoff data are not available; strikingly, the seasonal peak of evaporation usually observed in January is delayed by 3 months, and is significantly stronger than normal.

At this stage, and to summarize this first overview of our new SSS dataset, we have shown that the 2009-2014 period is characterized by a suite of alternating saltening and freshening phases in the NEB, that generate intense SSS anomalies (with magnitudes of 1 or more). The deficient runoff in 2009 appears as a possible candidate to explain the salty anomaly build-up seen from mid-2009 to early 2010. The sustained and increased saltening through 2010 is consistent with the deficient rainfall during summer 2010. The return to fresher-than normal conditions in late 2011 could be explained by both excess runoff and excess rainfall during 2011. The mid-2013 fresh anomaly is hard to explain, as we do not have any runoff estimate during this year and precipitation is only weakly in excess at that time. To quantitatively ascertain the respective role of the various components of freshwater flux in the observed variability of upper NEB salinity, as well as the role of ocean transports, we will use a simple mixed layer salinity budget in Section 4.

4. Mechanisms of NEB SSS variability

4.1 Salt budget computation

We use a simple mixed-layer salinity budget analysis in order to quantify the processes that drive SSS interannual variability in the BoB. The law of salt conservation applied to the oceanic mixed layer shows that near-surface salinity varies under the influence of freshwater exchanges with the atmosphere (evaporation, precipitation), continental runoff, horizontal advection by oceanic currents,

and exchanges with the subsurface layers (through vertical mixing, advection and entrainment). This method has been used in a few previous studies to investigate the processes driving salinity variability in the tropical Indian Ocean, either based on observations (Rao and Sivakumar 2003; Durand et al. 2013) or numerical models (Thompson et al. 2006; Vinayachandran and Nanjundiah 2009; Akhil et al. 2014). We can approximate the mixed layer salinity budget over the NEB domain as:

$$\frac{dS}{dt} = \frac{1}{hA} \left[\iint_{\text{lateral boundaries}} u_{\text{normal}} (S_{\text{boundary}} - S) ds + \iint_{\text{ocean surface}} (E - P - R) S ds \right] \quad (1)$$

where S is the box-averaged mixed-layer salinity, h is the mixed-layer thickness (prescribed, assumed to be constant in time and in space), A is the area of the box, u_{normal} is the horizontal current in the normal direction to the box boundaries (i.e. zonal component for the East and West boundaries, and meridional component for the North and South boundaries) considered positive when entering the box; S_{boundary} is the salinity at the boundary of the box; E is evaporation, P is precipitation and R is the freshwater flux of all rivers entering the box. The first term of the right-hand-side of (1) is the advection, computed as a two-dimensional integral along the vertical surfaces of the four boundaries of the box. The second term is a two-dimensional integral over the air-sea interface of the box. This equation neglects the space and time dependencies of the mixed-layer depth over the domain and assumes that the vertical exchanges of salt between the mixed-layer and the oceanic subsurface are of second order. This is clearly a limitation of our approach, but this practical choice is dictated by the absence of observational estimates of exchanges between the mixed-layer and the deeper oceanic layers in the BoB. We will further discuss the consequences of this approximation in Section 5.

As we are focusing on interannual SSS variability, we consider interannual anomalies of each of the terms relative to their seasonal climatology. The mixed-layer salinity budget Equation (1) applied to interannual mixed-layer salinity anomalies can be written as follows, assuming that higher order non-linear terms are negligible:

$$\frac{dS'}{dt} = \frac{1}{hA} \left[\iint_{\text{lateral boundaries}} \left[u_{\text{normal}} (S_{\text{boundary}} - S)' + u_{\text{normal}}' S_{\text{boundary}} - S \right] ds + \iint_{\text{ocean surface}} \left[(E' - P' - R') S + (E - P - R) S' \right] ds \right] \quad (2)$$

where \bar{x} and x' respectively denote the seasonal climatology and interannual anomaly of any variable x . Given the limited extent of available SSS data in our blended product, we have to operate some

simplifications in Equation (2) in order to make the problem tractable. No salinity data are indeed available along the eastern boundary of the NEB box (Fig. 3). As a result, the integral of advection term along this boundary cannot be estimated. This term is anyway expected to be small compared to the other two advection terms (through the southern and western boundaries of NEB box), owing to the limited extent of the eastern boundary (compared to the two others) and to the supposedly relatively sluggish circulation inducing weak tracers advection in the upper layers of the semi-enclosed Andaman Sea (Benshila et al. 2014). One more simplification dictated by the limited salinity data coverage concerns the advection of salinity anomalies by the seasonal currents (first advection term in Equation 2). It is not possible to compute a reliable estimate of the salinity anomalies all along the open boundaries of the NEB box, throughout our period. This term is therefore not accounted for either. Hence, the advection process of this simplified mixed layer salt budget only considers the second advection term of Equation (2) (advection of seasonal salinity by current anomalies). Finally, we computed the second freshwater forcing term (salinity trend induced by the change of background salinity) but it is negligible (not shown) and was thus not accounted for in the following analysis. In brief, the mixed layer salinity anomalies budget we use reads as follows, and neglects mixed layer depth space and time variations, exchanges with the subsurface, transport at the eastern box boundary, and advection of salinity anomalies by the climatological currents:

$$\frac{dS'}{dt} = \frac{1}{hA} \left[\iint_{\substack{\text{west and south} \\ \text{boundaries}}} u'_{normal} (S_{boundary} - S) ds + \iint_{\substack{\text{ocean} \\ \text{surface}}} (E' - P' - R') S ds \right] \quad (3)$$

We used interannual anomalies of the products described in Section 2 to estimate terms in equation (3): OSCAR currents, TropFlux evaporation, TRMM precipitation and our altimetric-derived discharge dataset for the Ganges, Brahmaputra and Irrawaddy rivers. We computed the time derivative of the salinity anomalies using a forward difference. We used the mixed layer depth observed estimate from de Boyer Montégut et al. (2004). It is defined as the depth where density exceeds the density at 10 m by an amount equivalent to a 0.2°C drop in temperature. Its climatological and spatially-averaged value over NEB box is 18 m. Note that on account of the limited availability of runoff data, we were only able to perform this budget over the 2009 – 2012 period.

4.2 Interannual SSS budget of NEB domain

Figure 7 (top) shows the time evolution of interannual SSS anomalies tendency derived from our observational gridded product over NEB box (black curve) and estimated from the simplified

mixed-layer salinity budget of Equation (3) (red curve), along with estimated contributions from advection (dashed green) and freshwater forcing (dashed blue). Figure 7 also features an estimate of the uncertainty of the observed interannual SSS tendency. This estimate was obtained as follows. The dominant source of error in the tendency estimate is the fact that some $2^\circ \times 2^\circ$ cells are regularly missing on trimonthly estimates. The intra-NEB box SSS variations indeed quite have a standard deviation of 1.02 over the entire dataset, i.e. they are much larger than instrumental errors, which are usually below 0.1. We thus used a Monte Carlo method to generate 1000 synthetic time series of salinity, by replacing any missing value by the box average plus a random variable with a centred normal distribution of 1.02 standard deviation. The spread of the temporal derivatives computed from those time series then allowed to estimate a 95% confidence interval on the value of $d(\text{SSS})/dt$. This confidence interval, typically of $\pm 0.15 \text{ month}^{-1}$ is similar to the one obtained by Da-Allada et al. (2013) in the tropical Atlantic basin, where freshwater forcing also plays a strong role in driving the SSS variations. The limits to this approach will be further discussed in Section 5.

The observed tendency (black curve) exhibits a succession of negative values (viz. freshening) before mid-2009 and during 2011, and positive events (viz. saltening) during the late 2009-late 2010 period as well as in the first half of 2012. The magnitude of the observed tendency reaches 0.3 per month (in absolute values) at the peak of both the freshening and saltening events. The evolution of SSS tendency estimated from the simplified mixed-layer salinity budget (red curve) displays a reasonable agreement with observed tendency in terms of timing of the freshening and saltening periods, with a correlation of 0.64 (Table 1). This implies that, despite its simplicity, the SSS budget defined by Equation (3) is reasonably closed. This legitimates a posteriori the assumptions we had to make in order to estimate this salt budget. The estimated mixed layer salinity budget however yields a SSS tendency that is somewhat smoother than observed, and an underestimated tendency magnitude during peak saltening and freshening periods. Despite this underestimation, the mixed layer salt budget tendency almost always lies within the bounds of the observed SSS tendency confidence interval; with a budget that only lies outside the bounds of the observational error bar in early 2010, mid-2011, and early 2012. This mismatch suggests that physical mechanisms not accounted for in our simple model, such as the influence of vertical physics, may play an important role during these periods: this will be further discussed in Section 5.

Table 1 provides an overview of the role of the various processes on the salt budget over the period. The freshwater forcing term correlates best with the observed SSS tendency, with a correlation of 0.68, indicating the primary role of freshwater forcing in driving the NEB average SSS. Both precipitation and runoff contribute to this over the entire period, with correlations to the observed

tendency of 0.55 and 0.42, respectively. On the other hand, while the advection term is sometimes comparable in amplitude to the freshwater forcing (Figure 7), it is only weakly correlated (0.13) to the observed storage over the entire period.

Over the entire period, freshwater forcing hence dominates large-scale SSS evolution in the NEB box. Let us now describe the budget throughout the period in more details. During summer monsoon (June-July-August), the total freshwater forcing term (E-P-R) is generally prominent (in 2010, 2011 and 2012). Consistently with our findings of Section 3, the contribution of river runoff dominates the contribution of precipitation in mid-2009, while the opposite holds true in mid-2010 (Figure 7). In mid-2011, both the river runoff and precipitation have a comparable influence. At some other times, particularly during the inter-monsoon seasons, the advection term dominates (March-April-May 2010 and September-October-November 2011). The relative contribution of zonal advection (through the western boundary of NEB domain) and meridional advection (through its southern boundary) is also highly variable: for instance the saltening advective peak of March-April-May 2010 is almost purely driven by the zonal advection, whereas the freshening peak of September-October-November 2011 is mostly driven by meridional advection with a minor contribution of zonal advection. Note that over the whole period, there is a slight tendency of meridional advection to be directly opposed to zonal advection. This can be simply explained by the flux formulation used for advection in our box model (Lee et al. 2004).

In order to identify more clearly the contribution of each of the forcing terms on the overall SSS evolution, we integrated Equation (3) during two successive periods of about one and a half year long: the ~ 1.7 unit saltening period from mid-2009 to late 2010, and the ~ 1.9 unit freshening period from late 2010 to early 2012. This diagnostic is similar to the one used by Durand et al. (2013) in the southern tropical Indian Ocean. The results of these two integrations are shown in Figure 8. As expected, the SSS change diagnosed by our mixed-layer model (red curves) broadly follows the observed change over both periods (black curve). In particular, the agreement between the modelled and observed SSS at the end of both integrations (in September-October-November 2010 and in December 2011 - January-February 2012) is quite good, despite an underestimation of both the overall saltening and freshening magnitude by our model (by about 0.5, for both cases).

Figure 8 also provides the time integral of the various forcing terms of SSS evolution. The 2009-2010 saltening event appears to be largely driven by fresh water forcing, and hence reflects the dominant control by this term over the entire period (Table 1). This term shows two periods inducing SSS increase (during the monsoons of 2009 and 2010), separated by a period when it induces hardly any change (from late 2009 to mid-2010). As seen in Section 3, the respective contributions of

precipitation and river discharge during these two successive monsoons are contrasted. During monsoon 2009, precipitation is close to normal whereas river discharge is deficient. During monsoon 2010, in contrast, precipitation is deficient and river discharge is slightly higher than normal. Globally these two terms act together to force a sustained saltening trend during two successive monsoons. The advection tendency terms show that the meridional component (through the southern boundary of NEB box) hardly plays any role, whereas the zonal component (through the western boundary) induces a marked saltening during the first half of 2010. Globally, during the first period of integration, the role of advection is secondary as compared to the role of the freshwater fluxes. From September-October-November 2010 to December 2011-January-February 2012, both freshwater and advective fluxes contribute to the freshening, with advective fluxes contributing about twice more (~ 0.9 unit) than freshwater fluxes (~ 0.5 unit). This hence illustrates that, while freshwater forcing tends to dominate over the entire period (Table 1), advection is not negligible at certain times. The freshening driven by the freshwater fluxes is most intense during monsoon 2011. It is explained by both excess rainfall and excess runoff as seen in Figure 6. Regarding advection, the zonal and meridional terms roughly cancel each other during the first part of the period (until mid 2011); then both terms contribute to freshen the domain (particularly so during September-October-November 2011), until the end of the integration period (early 2012).

5. Summary and discussion

The BoB upper ocean salinity stratification is believed to play a key-role in the Indian Ocean climate (e.g. Shenoi et al. 2002). Several observational studies have described the BoB SSS seasonal cycle and its driving processes over the past two decades (e.g. Rao and Sivakumar 2003; Chatterjee et al. 2012; Chaitanya et al. 2014). This seasonal cycle is closely linked to the monsoonal control of rainfall, river runoffs, and upper ocean circulation (Benshila et al. 2014; Akhil et al. 2014). Beyond this prominent seasonal cycle, there is also considerable interannual variability over the BoB. Precipitation (e.g. Gadgil 2003) and riverine freshwater supply to the bay (Papa et al. 2012) in particular vary significantly from year to year. The resulting BoB SSS interannual variability has however so far been little studied. The limited in situ measurements availability has indeed prevented the oceanographic community from assessing the interannual variability of BoB salinity over the past decade. During recent years, the BoB SSS observing system has drastically improved, now reaching a comparable status to that of the other tropical basins. As a result, it is now feasible to monitor the year-to-year basin-scale SSS variability in the BoB.

In this study, we assembled an unprecedented set of SSS observations over the BoB, including Argo profilers, a couple of repeated ship-of-opportunity buckets and XCTD transects, as well as RAMA

and OMNI moorings data. We merged these different datasets to obtain a $2^\circ \times 2^\circ$ x trimonthly product that satisfactorily covers the BoB at regional scale over 2009-2014. This product reveals a consistent area of marked year-to-year SSS variability, encompassing the north-eastern quarter of the basin. The typical SSS interannual anomaly magnitude ranges from 0.5 to 1 there. This magnitude is commensurate with signals observed in other highly variable regions of the tropical oceans, such as the equatorial Indian Ocean (Durand et al. 2013) or the far-eastern equatorial Pacific Ocean (Alory et al. 2012). The observed variability displays an 18-month long saltening period from mid-2009 to late 2010, followed by a 15-month long freshening period from late 2010 to early 2012. The late 2013 – early 2014 period is also fresher than normal.

Based on a simple mixed-layer salt budget, we identified the processes responsible for this year-to-year variability. The freshwater fluxes from oceanic precipitation and continental river runoff are most consistent with the observed NEB-average SSS interannual tendency, with a correlation of 0.68 (Table 1). Precipitation and river runoff both contribute to the observed saltening and freshening events. The precipitation and runoff however do not vary coherently: they reinforce each other during some years while they vary independently during others. Figure 9 shows precipitation anomalies during the contrasted monsoons of 2010 and 2011. There is a broad dry anomaly covering the NEB in June-July-August 2010, with a simultaneous wet anomaly in the southern half of the basin, probably related to the simultaneous La Niña event in the Pacific (Mujumdar et al. 2012) and/or to the negative Indian Ocean Dipole event in the equatorial Indian Ocean (Horii et al. 2013). One year later, the Southern-central part of the BoB experiences again anomalously wet conditions, while the NEB has turned to wetter-than-normal conditions to the North of 20°N ; the precipitation anomaly however does not appear to be organized at large scale, unlike in 2010, as the central part of NEB displays dry anomalies.

Our analysis suggests that horizontal advection, although secondary with a correlation of only 0.13 to the observed tendency over the entire period, can non-negligibly contribute to the salt budget at times. In particular, the anomalous advective processes exhibit a completely different behaviour in fall 2010 compared to fall 2011. The tropical Indian Ocean has an intrinsic mode of climate variability at interannual timescales, referred to as the Indian Ocean Dipole (henceforth IOD) (Reverdin et al. 1986; Saji et al. 1999; Webster et al. 1999). This mode consists of a basin-scale disruption of the seasonal structure of tropospheric wind, convection and upper ocean circulation, primarily in the equatorial basin. Based on ocean numerical models, Rao et al. (2002b), Thompson et al. (2006), and Jensen (2007) demonstrated the IOD impact on the BoB upper ocean circulation. They suggest that the BoB surface circulation is anomalously anticyclonic in fall during a positive

IOD. Since the background basin-scale SSS gradient is primarily oriented in the North-South direction during this season, with fresher water in the northern bay (Figure 1), this anomalous clockwise circulation pattern has the potential to induce fresh anomalies in the eastern bay (Thompson et al. 2006; Jensen 2007). Conversely, during a negative IOD event, the BoB circulation modelled by Thompson et al. (2006) is anomalously cyclonic during fall, and induces salty anomalies in the eastern bay. Figure 10 displays the anomalous surface circulation in the Bay of Bengal during the fall of 2010 (a negative IOD year) and 2011 (a positive IOD year). In line with past studies, OSCAR observed currents display a clear basin-scale cyclonic (resp., anticyclonic) sequence during the 2010 negative (resp. 2011 positive) IOD event. In September-October-November 2010, the anomalous flow across the southern boundary of the NEB domain is north-westward, and essentially parallel to the seasonal isohalines. This explains the minor effect of the advective processes on the 2010 SSS variability. In September-October-November 2011, in contrast, the flow is southward across NEB boundary, down the seasonal SSS gradient, which explains the strong freshening effect of advection during this period. Parampil et al. (2010) also observed that SSS variability in the BoB is significantly influenced by the variability of surface circulation. However, their study focused on short time and space scales (typically: the intra-seasonal timescales, and the mesoscale, respectively) while we focus here on SSS variability at much longer time and space scales (i.e. basin scale, interannual timescales).

Our simple mixed layer salt budget neglects vertical exchanges between the surface and subsurface through turbulent processes and advection. It however yields a SSS budget that lies within the bounds of the observational error on the SSS tendencies, hence suggesting that vertical physics do not prominently contribute to interannual SSS anomalies in the NEB over the period we analysed. This may seem contradictory with findings reported in the modeling study of Akhil et al. (2014), who concluded that vertical exchanges of salt between the mixed layer and the thermocline play an important part in the seasonal evolution of mixed-layer salinity in the northern BoB. This may be interpreted in two ways. Either processes responsible for the seasonal cycle and interannual anomalies of BoB SSS are indeed different, and vertical processes do not contribute as much to interannual SSS anomalies than to the seasonal cycle. Or there is a compensation between some of the neglected terms in our simple salt budget. The fact that our simple budget generally underestimates the magnitude of the most intense observed freshening and saltening spells in the BoB, could indeed be attributed to the lack of a proper representation of vertical physics. This limitation also prevents assessing the potential role of long baroclinic waves (coastal Kelvin waves, planetary Rossby waves), known to affect the thermohaline structure of Bay of Bengal at interannual

timescales (e.g. Rao et al. 2002a), on SSS interannual evolution. The BoB western boundary is also a region of strong interannual SSS variability (Figure 3a), in which our simple mixed layer salt budget does not perform well (not shown). The poor quality of remotely-sensed oceanic currents in coastal areas (e.g. Durand et al. 2009) could explain the inability of our simple budget to reproduce the SSS evolution there, since along-shore advection plays a key role in the seasonal freshening of the western BoB (Chaitanya et al. 2014; Akhil et al. 2014). Finally, the limited coverage of in situ salinity data also prevented us from estimating advection of anomalous salinity gradients by climatological currents. All these limitations related to the simplicity of our salt budget and to observational issues call for revisiting our conclusions using a more sophisticated numerical framework. A general ocean circulation model indeed takes the spatio-temporal variability of mixed-layer depth, vertical exchanges of salt/freshwater between the mixed layer and the deeper layers and all the horizontal advective terms explicitly into account. An investigation of the mechanisms at stake in driving the interannual SSS evolution in the Bay of Bengal using such a tool, with close comparisons to observed SSS variability derived in the current study, is therefore a promising perspective to the present study.

Keeping in mind the potential role of the BoB upper ocean salinity stratification on air-sea interactions (Shenoi et al. 2002, Neetu et al., 2012, and references therein), it would be interesting to explore how interannual variability of SSS can influence the interannual variability of the upper BoB heat budget and surface temperature. We believe that the present study opens the way for future research in this direction. The current observational density is indeed sufficient to observe large-scale seasonal anomalies. The observational dataset we have developed can hence be used as a ground truth for calibration/validation of present and future spaceborne salinity products (Subrahmanyam et al. 2013; Tang et al. 2014), and general circulation models of the Bay of Bengal. The current study also pleads not only for a sustained but also for an improved in situ observing system of the BoB salinity. Indeed, some areas (like the Andaman Sea) are not well sampled by existing observations, and current observations are not sufficient to confidently assess all the terms of the SSS balance.

Acknowledgements

We thank the three anonymous reviewers for their constructive comments on our paper. XCTD and bucket salinity observations are supported by the Ministry of Earth Sciences, through the Indian National Center for Ocean Information Services, Hyderabad, India. We thank the numerous people who spent a long time at sea collecting the salinity observations. Thermosalinograph data were collected and processed by the French SSS Observation Service (www.legos.obs-mip.fr/observations/sss). We sincerely thank the team efforts of NIOT technical and scientific staff

for providing continuous data from the OMNI moorings. We are thankful to Argo and RAMA programs for making their salinity data available to all. FD, FP, ML and JV are funded by Institut de Recherche pour le Développement (IRD). Part of this work was done when CAVS and FD visited the Indo-French Cell for Water Sciences (Joint International Laboratory IRD-IISc, Bangalore, India). Support from this laboratory is gratefully acknowledged. We acknowledge constructive comments by Debasis Sengupta.

References

Akhil VP, Durand F, Lengaigne M, Vialard J, Keerthi MG, Gopalakrishna VV, Deltel C, Papa F, de Boyer Montégut C (2014) A modeling study of the processes of surface salinity seasonal cycle in the Bay of Bengal. *J. Geophys. Res. Oceans*, 119, 3926-3947, doi: 10.1002/2013JC009632

Alory G, Maes C, Delcroix T, Reul N, Illig S (2012) Seasonal dynamics of sea surface salinity off Panama: the far Eastern Pacific Fresh Pool. *J Geophys Res* 117(C04028).doi:10.1029/2011JC007802

Benshila R, Durand F, Masson S, Bourdalle-Badie R, de Boyer Montégut C, Papa F, Madec G (2014) The upper Bay of Bengal salinity structure in a high-resolution model. *Ocean Modelling* 74:36-52

Bonjean F, Lagerloef GSE (2002) Diagnostic model and analysis of the surface currents in the tropical Pacific Ocean. *J Phys Oceanogr* 32(10):2938–2954

Chaitanya A V S, Lengaigne M, Vialard J, Gopalakrishna VV, Durand F, Kranthikumar C, Amritash S, Suneel V, Papa F, Ravichandran M (2014) Salinity measurements collected by fishermen reveal a “river in the sea” flowing along the east coast of India. *Bull Am Meteorol Soc.*, in press

Chatterjee A, Shankar D, Shenoi SSC, Reddy GV, Michael GS, Ravichandran M, Gopalakrishna VV, Rama Rao EP, UdayaBhaskar TVS, Sanjeevan VN (2012) A new atlas of temperature and salinity for the North Indian Ocean. *Journal of Earth System Sciences*. 121(3):559-593

Da-Allada C Y, Alory G, du Penhoat Y, Kestenare E, Durand F, Hounkonnou N M (2013) Seasonal mixed-layer salinity balance in the tropical Atlantic Ocean: Mean state and seasonal cycle. *J Geophys Res* 118.doi:10.1029/2012JC008357

de Boyer Montégut C, Madec G, Fischer AS, Lazar A, Iudicone D (2004) Mixed layer depth over the global ocean: an examination of profile data and a profile-based climatology. *J Geophys Res* 109(C12003).doi:10.1029/2004JC002378

de Boyer Montégut, C, J Mignot, A Lazar, and S Cravatte (2007) Control of salinity on the mixed layer depth in the world ocean: 1. General description, *J. Geophys. Res.*, 112, C06011, doi:10.1029/2006JC003953

de Boyer Montégut C, Durand F, Bourdallé-Badie R, Blanke B (2014) Barrier layer in the Arabian Sea during summer monsoon. *Ocean Dynamics*. doi:10.1007/s10236-014-0716-7

Dee D P et al (2011) The ERA-interim reanalysis: configuration and performance of the data assimilation system. *Q J R Meteorol Soc* 137:553-597. doi:10.1002/qj.828.

- Delcroix T, McPhaden MJ, Dessier A, Gouriou Y (2005) Time and space scales for sea surface salinity in the tropical oceans *Deep Sea Res., Part I* 52(5):787–813. doi:10.1016/j.dsr.2004.11.012.
- Durand F, Shankar D, Birol F, Shenoi SSC (2009) Spatiotemporal structure of the East India Coastal Current from satellite altimetry. *J Geophys Res* 114, C02013. doi:10.1029/2008JC004807.
- Durand F, Papa F, Rahman A, Bala SK (2011) Impact of Ganga-Brahmaputra interannual discharge variations on Bay of Bengal salinity and temperature during 1992 – 1999 period. *J. Earth Syst. Sci.* 120:859-872
- Durand F, Alory G, Dussin R, Reul N (2013) SMOS reveals the signature of Indian Ocean Dipole events. *Ocean Dynamics*. doi:10.1007/s10236-013-0660-y
- Furuichi T, Win Z, Wasson R J (2009) Discharge and suspended sediment transport in the Ayeyarwady River, Myanmar: centennial and decadal changes. *Hydrol Process* 23:1631–1641. doi:10.1002/hyp.7295
- Gadgil S, Joseph P V and Joshi N V (1984) Ocean–atmosphere coupling over monsoonal regions, *Nature*, 312, 141–143
- Gadgil S (2003) The Indian Monsoon and its variability. *Annual Review of Earth and Planetary Sciences* 31:429-467
- Girishkumar M S, Ravichandran M, McPhaden MJ (2013) Temperature inversions and their influence on the mixed layer heat budget during the winters of 2006–2007 and 2007–2008 in the Bay of Bengal. *J Geophys Res* 118. doi:10.1002/jgrc.20192
- Han W, McCreary JP, Kohler KE (2001) Influence of precipitation minus evaporation and Bay of Bengal rivers on dynamics, thermodynamics, and mixed layer physics in the upper Indian Ocean. *J Geophys Res* 106(C4):6895-6916
- Horii T, Ueki I, Ando K, Mizuno K (2013) Eastern Indian Ocean warming associated with the negative Indian Ocean dipole: A case study of the 2010 event. *J Geophys Res* 118:536-549. doi:10.1002/jgrc.20071
- Huffman GJ, Adler RF, Bolvin DT, Gu GJ, Nelkin EJ, Bowman KP, Hong Y, Stocker EF, Wolff DB (2007) The TRMM multisatellite precipitation analysis (TMPA): Quasi-global, multiyear, combined-sensor precipitation estimates at fine scales. *Journal of Hydrometeorology* 8(1):38-55
- Jensen T G (2007) Wind-driven response of the northern Indian Ocean to climate extremes. *Journal of Climate* 20:2978-2993. doi:10.1175/JCLI4150.1
- Jian J, Webster PJ, Hoyos CD (2009) Large-scale controls on Ganges and Brahmaputra river discharge on intraseasonal and seasonal time-scales. *Q J R Meteorol Soc*, 135:353–370. doi: 10.1002/qj.384
- Lee T, Fukumori I, Tang B (2004) Temperature advection: Internal versus external processes. *J Phys Oceanogr* 34:1936–1944.
- McPhaden MJ, Meyers G, Ando K, Masumoto Y, Murty VSN, Ravichandran M, Syamsudin F, Vialard J, Yu L and Yu W (2009) RAMA: The Research Moored Array for African-Asian-Australian Monsoon Analysis and Prediction. *Bull Am Meteorol Soc* 90:459-480

- Mujumdar M, Preethi B, Sabin TP, Ashok K, Saeed S, Pai DS, Krishnan R (2012) The Asian summer monsoon response to the La Nina event of 2010. *Meteorological Applications* 19:216–225
- Neetu S, Lengaigne M, Vincent EM, Vialard J, Madec G, Samson G, Ramesh Kumar MR, Durand F (2012) Influence of upper-ocean stratification on tropical cyclone-induced surface cooling in the Bay of Bengal. *J Geophys Res* 117(C12020).doi:10.1029/2012JC008433
- Papa F, Durand F, Rossow WB, Rahman A Bala SK (2010) Satellite altimeter-derived monthly discharge of the Ganga-Brahmaputra river and its seasonal to interannual variations from 1993 to 2008. *J Geophys Res*, 115(C12013).doi:10.1029/2009JC006075
- Papa F, Bala SK, Pandey RK, Durand F, Gopalakrishna VV, Rahman A, Rossow WB (2012) Ganga–Brahmaputra river discharge from Jason-2 radar altimetry:an update to the long-term satellite-derived estimates of continental freshwater forcing flux into the Bay of Bengal. *J Geophys Res* 117(C11021). doi:10.1029/2012JC008158
- Parampil SR, Gera A, Ravichandran M, Sengupta D (2010) Intraseasonal response of mixed layer temperature and salinity in the Bay of Bengal to heat and freshwater flux. *J Geophys Res* 115(C0500). doi:10.1029/2009JC005790
- Praveen Kumar B, Vialard J, Lengaigne M, Murty VSN, McPhaden MJ (2012) TropFlux: Air-Sea Fluxes for the Global Tropical Oceans - Description and evaluation. *Climate Dynamics* 38:1521-1543. doi:10.1007/s00382-011-1115-0
- Rao RR, Sivakumar R (2003) Seasonal variability of sea surface salinity and salt budget of the mixed layer of the north Indian Ocean. *J Geophys Res* 108.doi:10.1029/2001JC000907
- Rao SA, Gopalakrishna VV, Shetye SR, Yamagata T (2002a) Why were cool SST anomalies absent in the Bay of Bengal during the 1997 Indian Ocean Dipole Event ? *Geophys Res Lett* 29(0). doi:10.1029/2001/GL014645.
- Rao SA, Behera SK, Masumoto Y, Yamagata T (2002b) Interannual subsurface variability in the Tropical Indian Ocean with a special emphasis on the Indian Ocean Dipole. *Deep-Sea Research II* (49):1549-1572. doi:S0967-0645(01)00158-8
- Rao SA, et al. (2011) Modulation of SST, SSS over northern Bay of Bengal on ISO time scale. *J Geophys Res* 116. doi:10.1029/2010JC006804.
- Reverdin G, Cadet DL, Gutzler D (1986) Interannual displacements of convection and surface circulation over the equatorial Indian Ocean. *QJRMS* 112(471):43–67
- Roemmich D, Johnson GC, Riser S, Davis R, Gilson J, Owens WB, Garzoli SL, Schmid C, Ignaszewski M (2009) The Argo Program: Observing the global ocean with profiling floats. *Oceanography* 22(2):34–43. doi:10.5670/oceanog.2009.36
- Saji NH, Goswami BN, Vinayachandran PN, Yamagata T (1999) A dipole mode in the tropical Indian Ocean. *Nature* 401:360–363
- Sengupta D, Bharath Raj GN, Shenoi SSC (2006) Surface freshwater from Bay of Bengal runoff and Indonesian Throughflow in the tropical Indian Ocean. *Geophys Res Lett* 33(L22609). doi:10.1029/2006GL027573

Sengupta D, Bharath Raj GN, Anitha DS (2008) Cyclone-induced mixing does not cool SST in the post-monsoon north Bay of Bengal. *AtmosSci Let* 9:1-6.doi:10.1002/asi.162.

Shenoi SSC, Shankar D, Shetye SR (2002) Differences in heat budgets of the near-surface Arabian Sea and Bay of Bengal: Implications for the summer monsoon. *J Geophys Res* 107(C6). doi:10.1029/2000JC000679

Shesu RV, UdayaBhaskar TVS, Pattabhi Rama Rao E, Devender R, HemasundarRao T (2013) Open source architecture for web-based oceanographic data services. *Data Sci J* 12:47-55

Subrahmanyam B, Grunseich G, and Nyadjro ES (2013) preliminary SMOS Salinity Measurements and Validation in the Indian Ocean. *IEEE Transactions on Geoscience and Remotesensing*, 51. No.1:19-27

Tang, W., S. H. Yueh, A. G. Fore, and A. Hayashi (2014) Validation of Aquarius sea surface salinity with in situ measurements from Argo floats and moored buoys. *J. Geophys. Res. Oceans*, 119, 6171–6189, doi:10.1002/2014JC010101

Tanguy Y, Arnault S, Lattes P (2010) Isothermal, mixed, and barrier layers in the subtropical and tropical Atlantic Ocean during the ARAMIS experiment. *Deep Sea Res I* 57(4):501-517. doi:10.1016/j.dsr.2009.12.012

Thompson B, Gnanaseelan C, Salvekar PS (2006) Variability in the Indian Ocean circulation and salinity and its impact on SST anomalies during dipole events. *J Mar Res* 64:853-880

Venkatesan R, Arul Muthiah M, Ramesh K, Ramasundaram S, Sundar R, AtmanandMA (2013) Satellite communication systems for ocean observational platforms: Societal importance and challenges. *The Journal of Ocean Technology* 8(3): 47-73.

Vinayachandran PN, Nanjundiah RS (2009) Indian Ocean sea surface salinity variations in a coupled model. *ClimDyn*. doi:10.1007/s00382-008-0511-6.

Vinayachandran, PN, Neema CP, Mathew S, RemyaR (2012) Mechanisms of summer intraseasonal sea surface temperature oscillations in the Bay of Bengal. *J Geophys Res* 117(C01005).doi:10.1029/2011JC007433.

Webster PJ, Moore AM, Loschnigg JP, Leben RR (1999) Coupled ocean–atmosphere dynamics in the Indian Ocean during 1997–98. *Nature* 401:356–360. doi:10.1038/43848.

Figures and tables

Table 1. Correlation of the various components of the estimated mixed layer salt budget to the observed storage term in the NEB box

Total forcing	Freshwater	Advection	Precipitation forcing	River runoff forcing
0.64	0.68	0.13	0.55	0.42

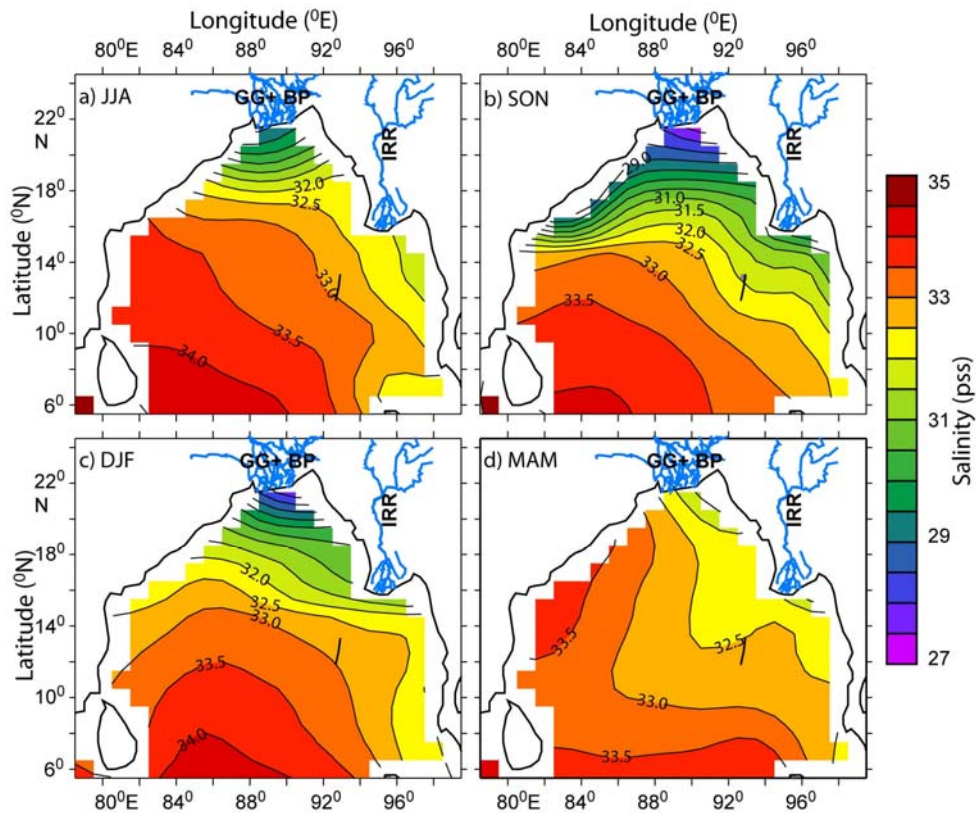


Figure 1. Seasonal evolution of SSS over the BoB from NIOA climatology (Chatterjee et al., 2012). Isocontours every 0.5. The three major rivers that flow into the Bay of Bengal (Ganges GG - Brahmaputra BP - Irrawaddy IRR) are shown as blue lines

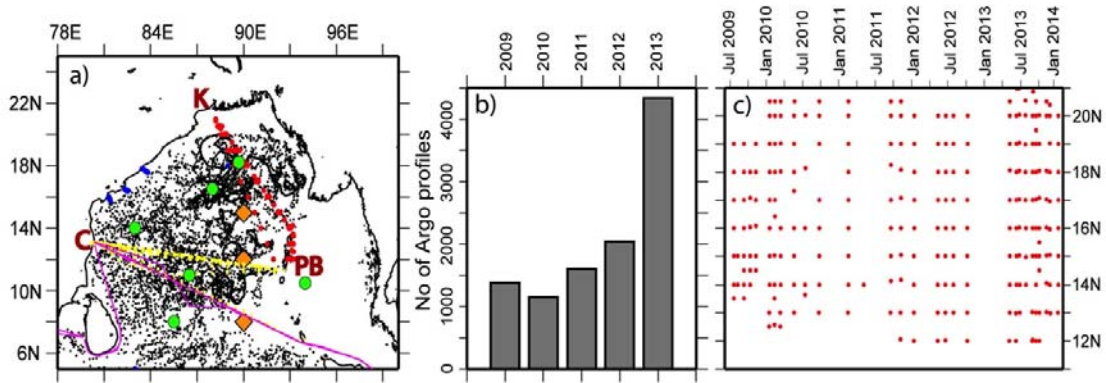


Figure 2. (a) Positions of in situ SSS observations over the BoB during 2009 – 2014 used in the present study, from the various sources of instruments: Argo profiles (black dots), XCTD profiles (red dots), bucket samples (yellow dots), thermosalinograph transects (pink), shipborne CTD stations (blue dots), RAMA moorings (orange diamonds) and OMNI moorings (green circles). (b) Evolution of the yearly number of individual Argo profiles from 2009 to 2013. (c) Latitude-time distribution of XCTD transects from 2009 to 2014, between Kolkata at 21°N (K) and Port Blair at 11°N (PB).

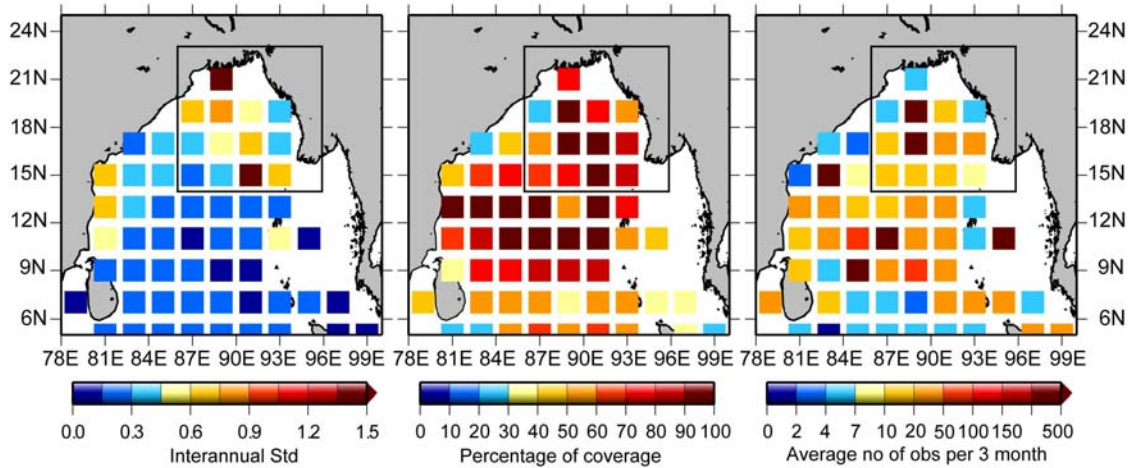


Figure 3. (a) Standard deviation of SSS interannual variability over 2009-2014 in our blended in situ product (in practical salinity scale). (b) Percentage of coverage of the blended product (i.e. ratio of the number of monitored seasons to the total length of the period). (c) Average number of individual observations for each three-month period, in each pixel. The black frame features the limits of the North-Eastern Bay (NEB) box (14°N-23°N, 86°E-96°E) that will be used subsequently.

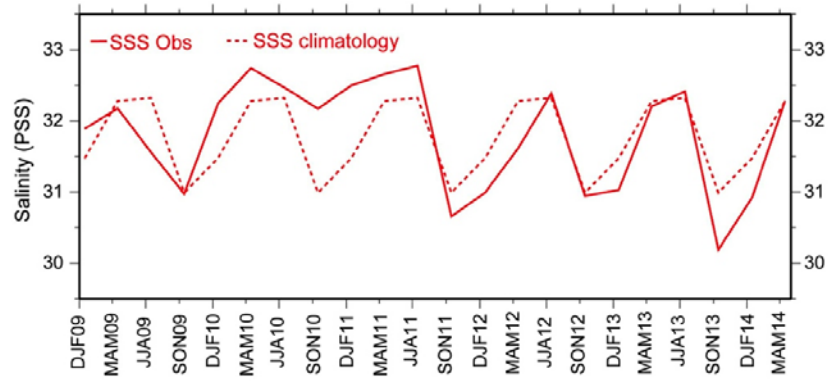


Figure 4. Trimonthly evolution of SSS averaged over the NEB box, from our blended product (solid red) and NIOA climatology (red dashes), from December 2009 to May 2014.

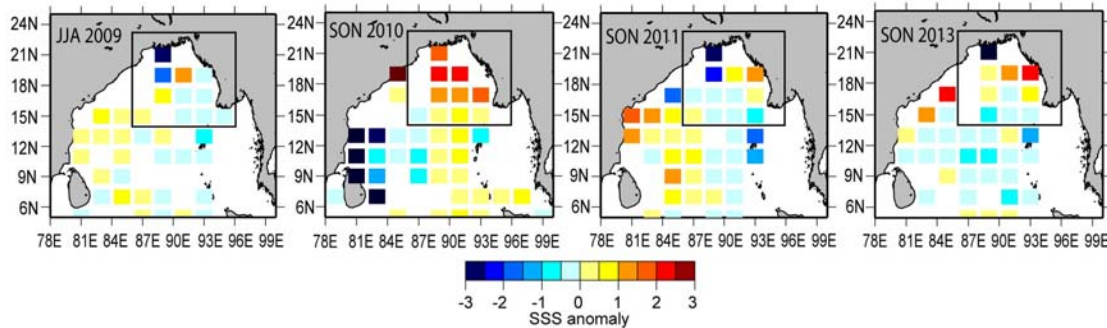


Figure 5. Map of interannual SSS anomalies at the peak of the fresh events (JJA 2009, SON 2011, SON 2013) and of the salty event (SON 2010). The limits of the NEB box are shown in black.

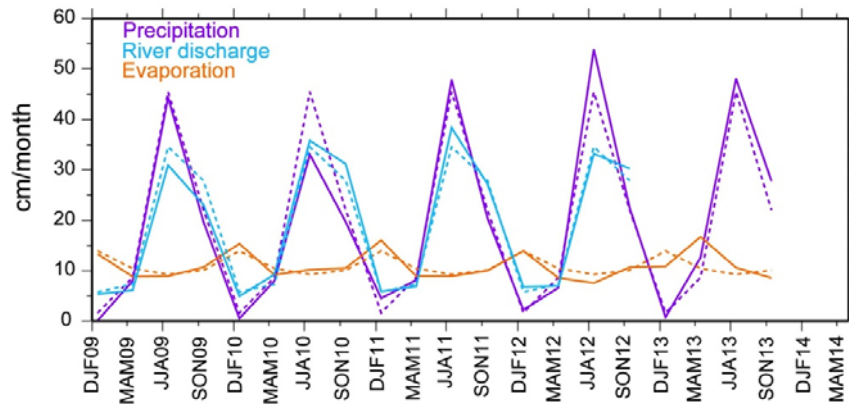


Figure 6. Trimonthly evolution of precipitation (purple solid), precipitation climatology (purple dashes), evaporation (orange solid), evaporation climatology (orange dashes), river discharge (blue solid), river discharge climatology (blue dashes), integrated over the NEB box (oceanic area only); the considered rivers are the Brahmaputra, Ganges and Irrawaddy (shown on Fig. 1). All fluxes are expressed in cm / month. Precipitation and evaporation climatologies were computed over 2009-2013 and the river discharge climatology was computed over 2009-2012.

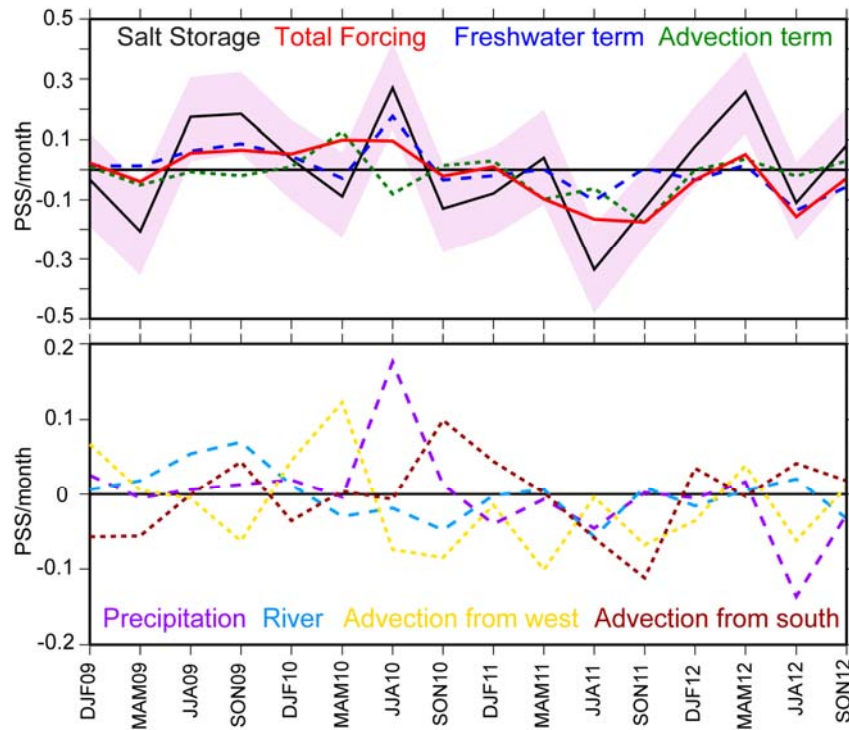


Figure 7. The top panel shows the trimonthly evolution of the tendency (i.e. time derivative) of the SSS interannual anomaly averaged over the NEB box, from December 2009 to November 2012, observed from our blended product (black) and estimated from our simple mixed-layer salt budget (red). The pink envelope features the error bar of the salt storage term (see text for details). The evolution of the various terms of the mixed-layer model is also shown, as follows: freshwater forcing in dark blue and horizontal advection in green. The bottom panel displays the corresponding evolution of the individual terms of the mixed-layer model, with precipitation term in purple, river runoff term in light blue, zonal advection in yellow, meridional advection in brown. The considered rivers are the Brahmaputra, the Ganges and the Irrawaddy (shown on Fig. 1). All terms are expressed in PSS (Practical Salinity Scale) / month.

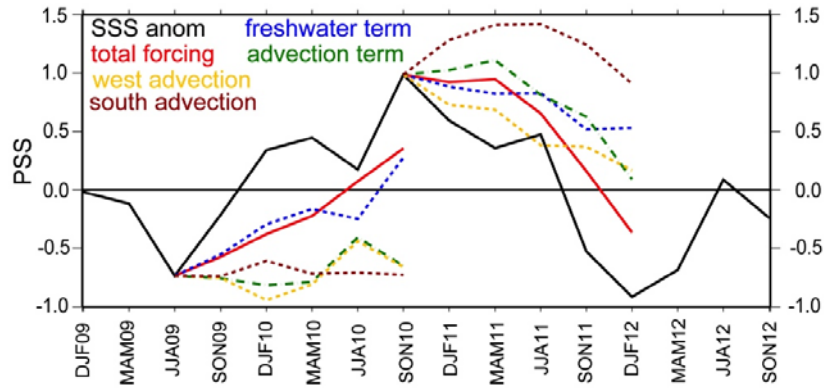


Figure 8. Trimonthly evolution of the observed SSS interannual anomaly averaged over the NEB box (black). The coloured lines show the SSS estimated from our simple mixed-layer salt budget, integrated over two periods, one starting in June-July-August 2009 and one starting in September-October-November 2010 (same colours as on Figure 7: contribution of freshwater forcing in dark blue, contribution of zonal advection in yellow, contribution of meridional advection in brown, contribution of total horizontal advection in green, the sum of all these terms in red).

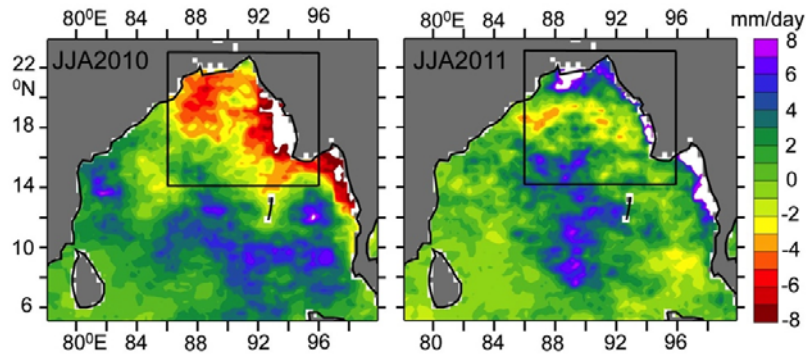


Figure 9. Precipitation interannual anomalies over the BoB in JJA 2010 (left) and JJA 2011 (right) (isocontours every 1 mm/day). The limits of NEB box are shown.

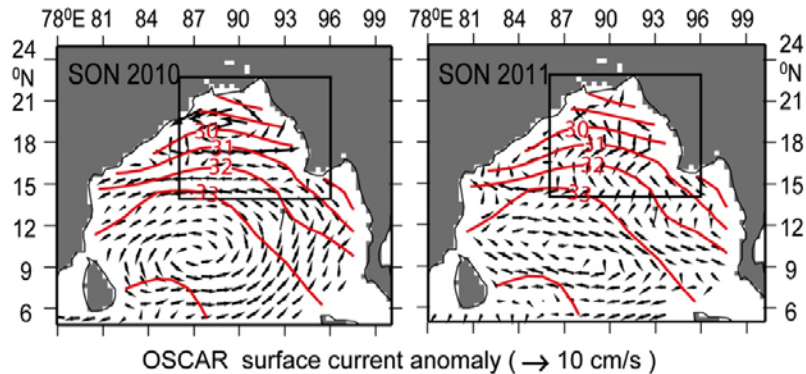


Figure 10. Surface current interannual anomalies over the BoB in SON 2010 (left) and SON 2011 (right). The seasonal SSS climatology from the NIOA atlas (Chatterjee et al., 2012) is superimposed on the current vectors (isocontours every 1 unit). The limits of NEB box are shown.